Remyelination reporter reveals prolonged refinement of spontaneously regenerated myelin

Berit E. Powers, Drew L. Sellers, Emilie A. Lovelett, Willy Cheung, Sheida P. Aalami, Nikolai Zapertov, Don O. Maris, and Philip J. Horner[1]

Department of Neurological Surgery and Institute for Stem Cell and Regenerative Medicine, University of Washington, Seattle, WA 98195

Edited by Fred H. Gage, The Salk Institute for Biological Studies, San Diego, CA, and approved January 23, 2013 (received for review June 28, 2012)

Neurological diseases and trauma often cause demyelination, resulting in the disruption of axonal function and integrity. Endogenous remyelination promotes recovery, but the process is not well understood because no method exists to definitively distinguish regenerated from preexisting myelin. To date, remyelinated segments have been defined as anything abnormally short and thin, without empirical data to corroborate these morphological assumptions. To definitively identify regenerated myelin, we used a transgenic mouse with an inducible membrane-bound reporter and targeted Cre recombinase expression to a subset of glial progenitor cells after spinal cord injury, yielding remarkably clear visualization of spontaneously regenerated myelin in vivo. Early after injury, the mean length of sheaths regenerated by Schwann cells and oligodendrocytes (OLs) was significantly shorter than control, uninjured myelin, confirming past assumptions. However, OL-regenerated sheaths elongated progressively over 6 mo to approach control values. Moreover, OL-regenerated myelin thickness was not significantly different from control myelin at most time points after injury. Thus, many newly formed OL sheaths were neither thinner nor shorter than control myelin, vitiating accepted dogmas of what constitutes regenerated myelin. We conclude that remyelination, once thought to be static, is dynamic and elongates independently of axonal growth, in contrast to stretch-based mechanisms proposed in development. Further, without clear identification, past assessments have underestimated the extent and quality of regenerated myelin.

regeneration | plasticity | internode

Nervous system disorders including traumatic injury, stroke, and neurodegenerative diseases such as multiple sclerosis induce loss of myelin and myelinating cells, interrupting signal conduction and depriving axons of trophic support essential for survival (1–4). Postmitotic oligodendrocytes (OLs) do not readily participate in remyelination (5, 6). Instead, glial progenitors, distinguished by expression of the α-receptor for PDGF and the chondroitin sulfate proteoglycan neural/glial antigen 2 (NG2) proliferate following demyelination and differentiate into remyelinating cells within a few weeks (7–10). Regeneration of myelin membranes restores saltatory conduction and supports axonal integrity, leading to partial recovery of function (3, 4, 11, 12). However, remyelination can fail during disease progression, and limited or abnormal myelin regeneration is thought to underlie chronic conduction deficits following trauma (11, 13, 14). Enhancing or substituting endogenous remyelination via pharmacological intervention or stem/progenitor cell transplantation has been a major, but unrealized, focus of clinical therapy development for decades (15–17).

There is much we do not understand about spontaneous remyelination, including the rate of OL regeneration, whether remyelinating cells select specific phenotypes or morphotypes of axons to ensheathe, and whether the initial number, thickness, or length of myelin internodes are dynamic. This is partly because no methods exist to definitively discriminate spontaneously regenerating myelin membranes from spared or degenerating sheaths. There are also no known molecular markers for regenerating myelin. Much of our understanding of myelin replacement is instead derived from interpretation of small-field EM or quantification of indirect histological markers (14, 18–21). Groundbreaking EM studies in the 1960s and 1970s confirmed the phenomenon of central remyelination, revealing thin, loosely wrapped sheaths that resembled immature myelin (18) as well as abnormally short myelin internodes (20) a few weeks after demyelination. Since that time, abnormally thin or short sheaths have been presumed to represent regenerated myelin. Investigators still commonly use these morphological characteristics alone to identify and study remyelination (11, 19, 20, 22).

This approach has likely limited understanding of the endogenous regeneration process. Measuring sheath length or thickness does not empirically determine whether a myelin sheath is new, degenerating, or preserved. Inappropriately thin and shortened myelin segments also result from partial demyelination of developmentally generated sheaths (23–25). Furthermore, it has long been suspected that internodes with normal proportions could be formed by remyelinating cells (19). If regenerated sheaths were able to thicken or elongate over time, for example, they would be morphologically indistinguishable from normal myelin. In short, we cannot be sure that all abnormally thin or short myelin is regenerated, nor that all sheaths with normal dimensions are a product of development rather than regeneration. Myelin sheath dimensions affect signal conduction speed considerably, and sluggish conduction following insult has been attributed in part to irregular remyelination (11, 12, 26–29). A better comprehension of these fundamentals is essential in guiding a new understanding of spontaneous myelin regeneration and therapeutic approaches to demyelinating disorders.

To follow the evolution and maturation of regenerating myelin membranes, we used a model of spinal cord contusion injury known to cause significant partial demyelination of spared axons followed by spontaneous remyelination (28). We targeted reporter expression to the membranes of proliferating $NG2^+$ glial progenitors via postinjury retrovirus injections in a mouse strain that ubiquitously expresses membrane-bound GFP following Cre recombination (30). Our findings revealed dynamic remodeling of myelin internodes over time and challenge several morphological dogmas in regard to how regenerated myelin forms.

Results

Cre-Mediated Recombination Is Evident in Premyelinating Glial Progenitors Acutely After Injury. To generate a reporter system for remyelination, three essential elements were combined (Fig. S1). (*i*) Remyelinating cells were specifically targeted by a combination of the NG2 promoter (31) and a retrovirus that integrates DNA into the host genome only during mitosis (32). We chose the NG2 promoter because it is expressed by resident glial progenitors that can produce OLs and Schwann cells (SCs) after injury as well as by infiltrating peripheral SCs that participate in central remyelination

Author contributions: B.E.P. and P.J.H. designed research; B.E.P., D.L.S., E.A.L., W.C., S.P.A., N.Z., D.O.M., and P.J.H. performed research; B.E.P. and D.L.S. contributed new reagents/analytic tools; B.E.P. and D.O.M. analyzed data; and B.E.P., D.L.S., and P.J.H. wrote the paper.

The authors declare no conflict of interest.

This article is a PNAS Direct Submission.

[1]To whom correspondence should be addressed. E-mail: phorner@uw.edu.

This article contains supporting information online at www.pnas.org/lookup/suppl/doi:10.1073/pnas.1210293110/-/DCSupplemental.

(10, 33–35). The promoter and its efficient targeting of NG2$^+$ glial progenitors has been fully characterized previously (31). (*ii*) We tracked the remyelination process over a long postinjury period by using the Cre-loxp system to induce stable reporter gene expression. (*iii*) Clear visualization of myelin membranes was accomplished by using a membrane-targeted reporter, as most cytoplasm is extruded from compact myelin (36). We used a mouse strain that ubiquitously expresses membrane-targeted tandem dimer Tomato (mT) but switches to membrane-targeted GFP (mG) following Cre-mediated recombination (30). We injected virus into spinal cords of reporter mice 6 d after moderate thoracic contusion injury, when many NG2$^+$ progenitors that go on to remyelinate are thought to proliferate (15, 34).

To ensure that virus targeted proliferating glial progenitor cells rather than spared, postmitotic OLs, we examined spinal cord sections of contused mice for mG expression 5 d post virus (DPV) injection. At this time point, recombination in infected cells should have induced a switch from mT to mG expression (30), but myelin regeneration was unlikely to have begun (18). We therefore expected to find mG$^+$ cells, but not mG$^+$ myelin sheaths. Numerous perilesional mG$^+$/mT$^-$ cells were observed at 5 DPV (Fig. 1*A*). Some mG$^+$ cells were highly NG2-immunopositive and exhibited characteristic OL progenitor cell morphology (Fig. 1*B*). As expected, no mG$^+$ myelin was observed at 5 DPV. To further establish that mG$^+$ populations were not composed of postmitotic cells and eliminate the possibility that preexisting myelin was labeled, animals received a single i.p. injection of the mitotic marker BrdU concurrent with virus injection. We found at 5 DPV that mG$^+$ cells were BrdU$^+$, indicating that they had undergone division at the time of virus injections (Fig. 1*C*).

We examined tissue sections at 14 DPV to determine whether cells labeled 6 d postinjury had commenced regeneration of myelin. mG$^+$ cells showed evidence of differentiation: they exhibited complex multiprocess morphologies and APC$^+$ cell bodies characteristic of premyelinating OLs (Fig. 1*D*). However, no mG$^+$ myelin was visible at 14 DPV. Taken together, these results confirm that the virus infected dividing NG2-expressing glial progenitors, and not postmitotic, myelinating OLs. Furthermore, we confirm that regenerated myelin membranes take at least 2 wk to initially form (18).

Regenerating Myelin Sheaths Are Evident 1 mo After Virus Injection. To determine whether the reporter system targeted regenerating myelin membranes, we examined longitudinally sectioned spinal cords of injured mice killed at 1 mo post virus (MPV) injection, when remyelination was predicted to be well under way (18). Sections contained OL-associated mG$^+$ sheaths (Fig. 2), which were hollow as expected (Fig. 2*D*) and filled with neurofilament (NF)$^+$ axons (Fig. 2*F*). Sheaths exhibited contactin-associated protein 1 (CASPR1)$^+$ paranodes at each end, indicating a reconstituted nodal structure (Fig. 2*F*). GFP signal within OL-regenerated sheaths colocalized with the marker of compact myelin, myelin basic protein (MBP; Fig. 2*E*). OL somata were remotely connected to multiple myelin sheaths by fine processes. The myelin reporter allowed us to map many of the mG$^+$ myelin sheaths to mG$^+$ cell bodies immunopositive for the OL marker APC (Fig. 2*C*). Physical parameters (length and thickness) of mG$^+$ regenerated myelin were quantified by confocal microscopy (Figs. 3 and 4). Other mG$^+$ internodes exhibited an mG$^+$ soma with DAPI$^+$ nucleus juxtaposed to the exterior of each sheath (Fig. 5 *A* and *B*) and immunopositivity for P0 and periaxin (Fig. 5 *D* and *E*), characteristic of peripheral myelin produced by SCs.

By using confocal microscopy, we observed coincident but also nonoverlapping regions of mG and MBP indicating reporter labeling of noncompact and compact myelin. To determine whether reporter-labeled regenerated myelin was multilamellar and compact, we performed immuno-EM on tissue sections stained with an anti-GFP primary, followed by a secondary antibody conjugate made with quantum dot nanocrystals (Qdots; ~4 × 10 nm in length) that fluoresce under UV light and are also visible by EM. We confirmed GFP/Qdot colocalization by confocal microscopy (Fig. 2*G*) and visualized Qdots of the appropriate size (4 × 10 nm) labeling compact, multilamellar myelin in injured mice at 3 MPV (Fig. 2 *H*–*L*).

Quantitative Characterization of Myelin Sheaths in Uninjured Controls. To establish a baseline for our experiments in the injury model, we quantified the structural characteristics of normal myelin in uninjured reporter mice. Animals received a single thoracic microinjection of virus at postnatal day (P) 4 or P5, when many NG2$^+$ progenitor cells undergo proliferation before differentiating into myelinating cells. Animals were killed as age-matched, uninjured adult controls. They exhibited mG$^+$ myelin sheaths bounded by CASPR1$^+$ paranodes throughout the thoracic white matter (Fig. 3*A*). We quantified myelin dimensions by using confocal microscopy. The mean internode length of developmentally generated myelin in thoracic segments 8 to 11 was 214 ± 97 μm, with a range of 28 to 495 μm (Fig. 3*B*). Consistent with previous EM studies (20, 37), sheath length and width were positively correlated (Fig. 3*E*). We also determined g-ratio, the relationship of axonal diameter to

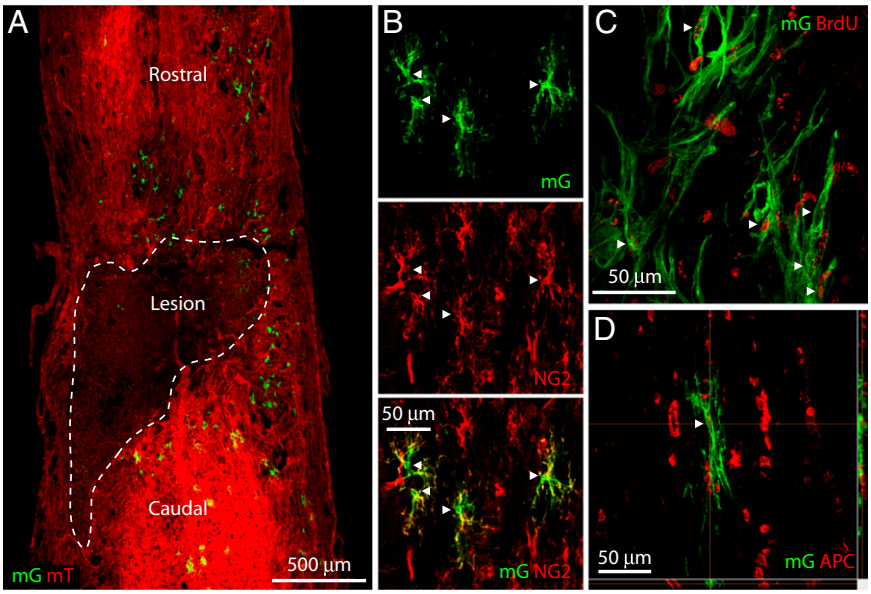

Fig. 1. Cre-mediated recombination is evident in glial progenitors, but not in myelin early after injury, demonstrating targeted labeling of remyelinating cells, and not preexisting myelin. (*A*) A low-power, merged confocal *z*-series depicts perilesional mG$^+$ cells 5 DPV, but, as expected, no mG$^+$ myelin sheaths are yet evident. (*B*) Some mG$^+$ cells are highly NG2$^+$ with classic glial progenitor morphology (arrowheads). (*C*) mG$^+$ cells exhibited BrdU$^+$ nuclei 5 DPV (arrowheads). More than 80% were BrdU$^+$, although some stained weakly, indicating likely BrdU dilution with multiple cell divisions. Cells in *C* resemble immature SCs. (*D*) At 14 DPV, still no mG$^+$ sheaths were evident, but many cells exhibited complex elongated morphology and APC$^+$ somata characteristic of premyelinating OLs.

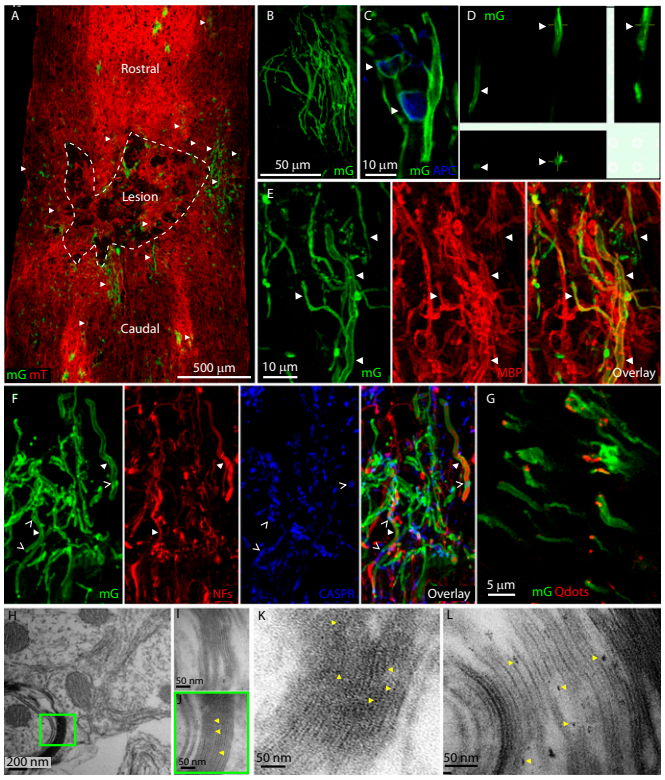

Fig. 2. Regenerated myelin sheaths are evident by 1 MPV. (*A*) A low-power, merged confocal *z*-series depicts regenerated myelin near the lesion, labeled with the mG reporter (arrowheads) at 1 MPV. (*B*) Higher magnifications demonstrate that regenerated myelin (mG^+) is abnormally short (~50 μm; merged *z*-series image). (*C*) Single *z*-plane from *B* reveals APC^+/mG^+ somata (arrowheads) adjacent to mG^+ myelin sheaths, typical of OL morphology. (*D* and *F*) Each sheath is hollow when imaged in cross section (*D*, single *z*-plane, arrowheads), and filled with an NF^+ axon (*F*, arrowheads). (*E* and *F*) mG^+ sheaths are MBP^+ (*E*, arrowheads) and exhibit $CASPR^+$ paranodes at both ends (*F*, carets). (*G*) Specific Qdot localization is shown at the cut ends of mG^+ sheaths at the surface of this transverse spinal cord section, which was imaged on a confocal microscope before processing for EM. (*H–L*) EM images demonstrate unlabeled myelin (*I*) and Qdot labeling (yellow arrowheads; ~4 × 10 nm in length) of compact, multilamellar regenerated myelin at various magnifications (*H* and *J–L*) in mice killed at 3 MPV.

total fiber diameter (including myelin), which is commonly used as a measure of myelin thickness. The g-ratios we obtained (mean, 0.77 ± 0.11) were consistent with previous EM studies in adult mouse spinal cord (38, 39).

Reporter-Labeled SCs Selectively Ensheathe Large Axons, Accounting for One Third of Regenerated Sheaths at 1 MPV. We used confocal microscopy to quantify mG^+ myelin and ensheathed axonal parameters at 1 MPV (Fig. 3 *B–E*). Regenerated sheaths were significantly shorter than average control sheaths by one-way ANOVA: average OL-regenerated sheath length was 38 ± 21 μm, only 18% of average uninjured length (range, 10–127 μm; $P < 0.001$), whereas mean SC sheath length was 92 ± 42 μm, 43% of normal (range, 36–220 μm; $P < 0.001$; Fig. 3*B*). OL-regenerated sheaths were also significantly shorter than those of SCs ($P < 0.001$; Fig. 3*B*).

Surprisingly, mean g-ratio was not significantly different between OL-regenerated sheaths (0.78 ± 0.10) and controls (0.77 ± 0.11; $P > 0.05$; Fig. 3*C*). Previous reports have relied upon thin sheaths as a hallmark of regenerated myelin (14, 20, 22, 40), but our data indicate that it can be surprisingly similar in thickness to normal myelin. In contrast, mean mG^+ SC g-ratio was significantly lower (0.70 ± 0.12; $P < 0.05$; Fig. 3*C*) compared with uninjured central control sheaths, demonstrating that SCs retain their capacity to produce thicker myelin than OLs (41) even within the setting of postinjury central remyelination.

Strikingly, we found that SCs and OLs myelinated separate axonal populations at 1 MPV (Fig. 3*D*). Regenerated OLs ensheathed predominantly small axons (97% were 0.5–2 μm in diameter), whereas SCs selectively ensheathed larger caliber axons (50% were >2 μm in diameter; only 5% were <1 μm thick, with a range of 0.90–0.96 μm). SCs are known to target axons with diameters of 1 μm or greater in the periphery and in central remyelination (19, 42). However, our data further indicate that regenerated OLs predominantly avoid or are outcompeted for ensheathment of large axons early after injury, providing a first look at how remyelinating OLs also initially target axons based on caliber. Further, our data confirm a known positive correlation between sheath length and total fiber diameter in normal myelin (37) and demonstrate that it occurs in regenerated myelin, even within the population of extremely short mG^+ segments regenerated by OLs (Fig. 3*E*). Last, 36% of mG^+ myelin was SC-generated, indicating substantial contribution of peripheral-like sheaths to central remyelination.

SC-Regenerated Myelin Thickens Substantially Over Time. To examine the maturation of regenerating SC myelin, we used confocal microscopy to quantify sheath and axonal dimensions at 1, 3, and 6 MPV. Mean length of SC remyelination did not change significantly between 1 and 6 MPV by one-way ANOVA (1 MPV, 92 ± 42 μm; 3 MPV, 100 ± 27 μm; 6 MPV, 89 ± 23 μm; $P > 0.05$). However, mean g-ratio decreased significantly at 3 and 6 MPV (0.55 ± 0.09 and 0.54 ± 0.07, respectively) compared with 1 MPV (0.70 ± 0.12; $P < 0.001$), indicating a substantial thickening of SC myelin over time (Fig. 5), to a degree that is normal for peripheral but abnormally thick for central myelin (42). SC sheaths also attained a complex morphology by 6 MPV, complete with the Schmidt–Lanterman incisures typical of peripheral myelin (Fig. 5*C*). This morphological identifier reflects the significant advantage of using a membrane reporter for the purpose of studying myelin regeneration.

OL-Regenerated Myelin Ensheaths Larger-Caliber Axons over Time and Elongates Independently of Axonal Growth. To track the evolution of OL-regenerated myelin, we examined mG^+ sheath dimensions and axonal parameters from 1 to 6 MPV. In contrast to 1 MPV, OL-regenerated myelin ensheathed small- and large-caliber axons at 3 and 6 MPV (Fig. 4 *A* and *B*). The percentage of axons >2 μm in diameter ensheathed by regenerated OLs increased from 4% at 1 MPV to 22% and 20% at 3 and 6 MPV, respectively (Fig. 4*B*).

Strikingly, the mean length of OL-regenerated myelin increased progressively between 1 and 6 MPV (1 MPV, 38 ± 21 μm; 3 MPV, 51 ± 29 μm; 6 MVP, 62 ± 24 μm; Fig. 4*C*). The effect was particularly apparent on small-caliber axons (0.5–1 μm in diameter), where there was considerable overlap of control values with regenerated sheath lengths at 3 and 6 MPV (control, mean, 96 ± 54 μm; range, 28–204 μm; 1 MPV, mean, 32 ± 19 μm; range, 10–111 μm; 3 MPV, mean, 56 ± 30 μm; range, 13–194 μm; 6 MPV, mean, 72 ± 30 μm; range, 37–166 μm). Significant mG^+ sheath elongation was also apparent on medium caliber axons (1–2 μm diameter), but not on large (>2 μm) axons. Interestingly, the positive correlation between sheath length and axon diameter evident at 1 MPV was reversed by 6 MPV (1 MPV, Pearson $r = 0.12$; 6 MPV, Pearson $r = -0.31$). Our data indicate that, whereas OL remyelination on small- and medium-caliber axons elongates progressively, remyelination of the largest axons is initiated later and does not appear to lengthen significantly. Perhaps myelin sheath refinement on axons with a large surface area takes longer than 6 mo or there could be a functional reason for them to remain short.

We also examined the thickness of regenerated OL myelin over time (Fig. 4*D*). As we expected, mean g-ratio was significantly higher at 3 MVPI (0.82 ± 0.09), indicating thinner myelin

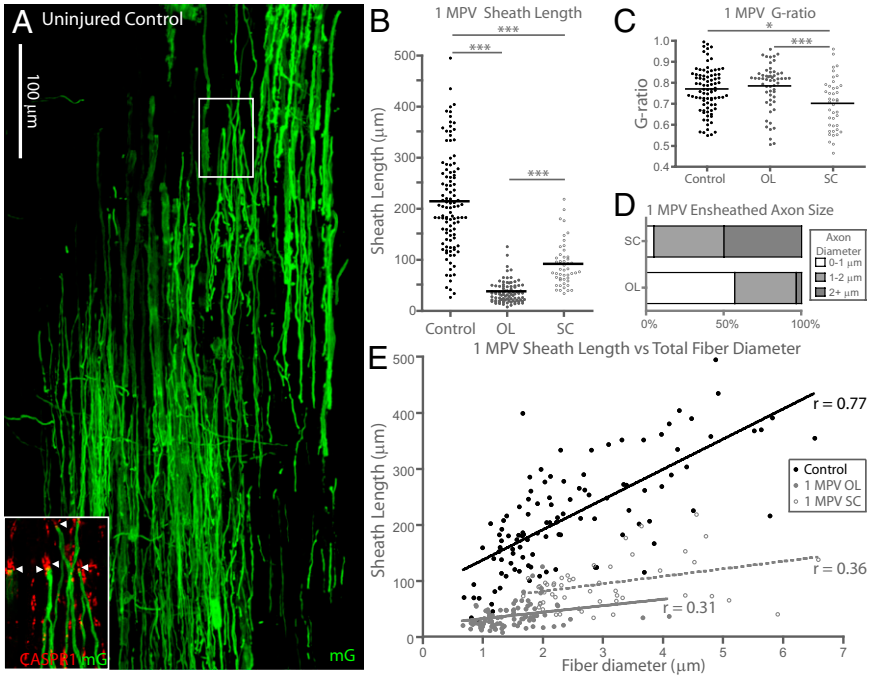

Fig. 3. At 1 MPV, OL- and SC-regenerated sheaths are significantly shorter than controls and myelinate separate axonal populations. (*A*) Merged confocal *z*-series depicts thoracic segment 10 uninjured control spinal cord containing a mix of thick and thin mG$^+$ myelin sheaths. (*Inset*) CASPR1$^+$ paranodes at sheath ends. (*B*) Mean regenerated sheath length is significantly shorter than controls; OL-regenerated sheaths are also significantly shorter than SC sheaths. (*C*) Mean OL-regenerated g-ratio is similar to controls whereas SC g-ratio is significantly lower than both, indicating thicker myelin. (*D*) Regenerated OLs myelinate a high proportion of small-caliber axons and few large axons; the reverse is true of regenerated SCs. (*E*) Sheath length and total fiber diameter are positively correlated in all groups (control, $P < 0.0001$; OL, $P < 0.01$; SC, $P < 0.05$; $^*P < 0.05$ and $^{***}P < 0.001$).

compared with controls (0.75 ± 0.10; $P < 0.001$). It is important to note that confocal analysis of myelin thickness may not give exact myelin measurements as seen by high-contrast EM of myelin membranes. Nevertheless, despite the reliance on a correlative distribution of mGFP along compact myelin, we find remarkable consistencies with g-ratios we have reported with EM (28). We confirm our previous EM studies and find that the mean g-ratio (and therefore myelin thickness) was not significantly different

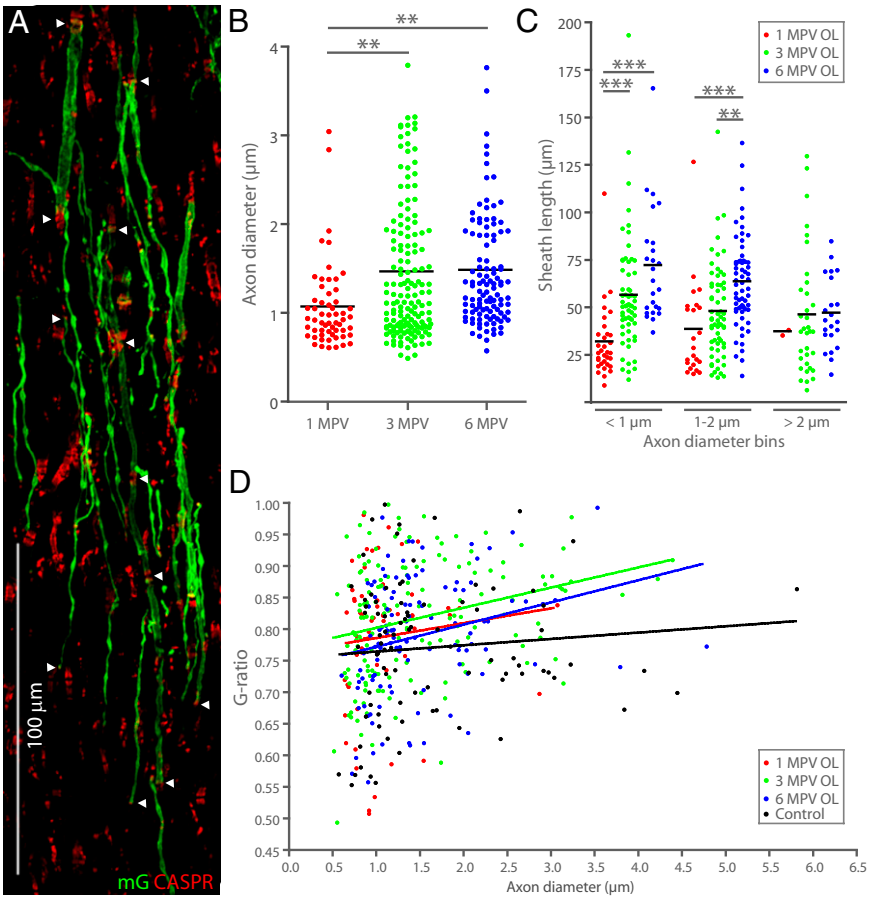

Fig. 4. OL-regenerated sheaths exhibit postinjury remodeling. (*A*) OL-regenerated sheaths at 3 MPV. Arrowheads indicate CASPR$^+$ paranodes. (*B*) Average axon diameter ensheathed by regenerated OLs is significantly larger at 3 and 6 MPV than at 1 MPV. (*C*) On small and medium-caliber axons, OL-regenerated sheaths increase in length over time. Small-caliber axons develop longer myelin sheaths than large-caliber axons, reversing the normal relationship between axon diameter and internodal length. Long, thin sheaths and short, thick sheaths can be seen in *A*. (*D*) G-ratios of regenerated and uninjured control myelin overlap considerably at all time points following injury ($^{**}P < 0.01$, $^{***}P < 0.001$).

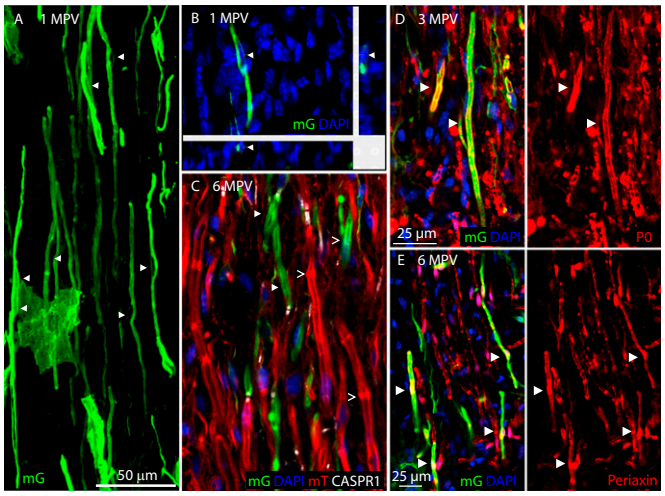

Fig. 5. mG$^+$ SC-regenerated sheaths are evident 1, 3, and 6 MPV. (*A*) Merged confocal *z*-series depicts mG$^+$ SC sheaths at 1 MPV. Arrowheads indicate somata hugging each sheath, typical of SC morphology, which are DAPI$^+$ as seen in *B* (arrowheads in single *z*-plane). (*C* and *D*) By 3 and 6 MPV, SC myelin gains complexity. (*C*) Arrowheads indicate a double-layered appearance in mG$^+$ sheaths in a single *z*-plane. Carets indicate Schmidt–Lanterman incisures, characteristic of mature SC myelin. mT$^+$ SC-regenerated myelin is also evident. SC-regenerated sheaths are (*D*) P0$^+$ and (*E*) periaxin$^+$.

between control and regenerated myelin at 1 MPV (0.78 ± 0.10; $P > 0.05$) or at 6 MPV (0.79 ± 0.09; $P > 0.05$). These g-ratio values may reflect a developmental-like evolution of remyelination: initial loose ensheathment by a few myelin lamina at 1 MPV, followed by compaction of the lamina by 3 MPV, and then gradual thickening of myelin (addition of membrane wraps) to reach average control levels by 6 MPV. Perhaps most striking is that, when g-ratios are binned by axonal size (<1 μm, 1–2 μm, <2 μm), there are no significant differences by one-way ANOVA between experimental groups and controls at any time point interrogated (Fig. 4*D*).

Discussion

This study prospectively distinguishes between regenerating and preexisting myelin sheaths to quantify the time course and physical development of spontaneously regenerated myelin. Contrary to dogma, we find that remyelinated segments with abnormal proportions are transient, except on the largest surviving axons. Most eventually attain lengths and thicknesses within the normal range, indicating that endogenous remyelination is not typically anemic as was previously assumed. Furthermore, our data demonstrate that remyelination can elongate independently of axonal growth, in contrast to stretch-based mechanisms proposed in development (43, 44). We conclude that the full extent of remyelination cannot be assessed by morphological criteria alone. Further mechanistic insights into the regenerative process will require empirical categorization of remyelinating membranes with the use of similar reporter strategies.

Our data also establish an association between the subspecies of remyelinating cell and the caliber of axon it ensheathes. In parallel with normal peripheral myelination (45), SCs only remyelinated axons larger than 1 μm in diameter. OLs, however, specifically selected against or were outcompeted for large axons at early time points, in surprising contrast to normal development. OLs, which myelinate many axons simultaneously, could initially be limited in myelinating multiple large surface areas by membrane production rates or inadequate access to necessary metabolites, whereas SCs may be more suitable to the task because they generate only a single internode each (46). Alternatively, an SC/OL fate choice could be induced in endogenous central progenitors by demyelinated axons of a particular size (10). Recent studies demonstrate that the myelinating potential of OLs is actively regulated by axons (47) and that caliber-based selection of axons could be mediated via axoglial integrin signaling (48). In either case, it is clear that SCs are capable and perhaps even essential for quick restoration of saltatory conduction and neuroprotection to large axons, at least in the first stages of recovery from trauma. Conversely, the inability of SCs to myelinate small axons makes OLs indispensable in central remyelination.

Confirming earlier reports (18, 20), OL-regenerated myelin was initially very short compared with normal myelin. SC-regenerated sheaths were longer and thicker than their OL counterparts, but still only approximately half as long as control sheaths. Whereas SC sheath length was static over time, OL-regenerated sheaths elongated on small and medium-sized axons, remarkably reaching the normal range of intact, developmental controls. Furthermore, after 6 mo, we did not find extremely short myelin internodes of 20 μm or less, which were initially common. The temporal loss of short internodes indicates that some myelin was likely pruned over time, to make room for elongation of neighboring sheaths. Although we do not have direct evidence of this phenomenon, myelin plasticity must be occurring and warrants future exploration. Last, our data suggest a previously underappreciated level of plasticity not only in myelin membranes, but also in reconstituted nodal structures.

The most striking finding of this study is the low abundance of abnormally thin regenerated myelin, challenging a key assumption in the field. Previously, regenerated sheaths have been classified in pathological conditions as falling into a very high g-ratio range of 0.9 to 1.0 with thicknesses less than ~20% of developmental myelin (14, 19, 22). Many studies have reported a high prevalence of very thin myelin surrounding lesion zones even years after spinal cord injury (14, 22). Given our observations, it is unlikely that a majority of long-standing, abnormally thin myelin in zones of pathologic conditions such as trauma, stroke, or disease is the result of incomplete myelin regeneration. It may instead be derived from preexisting myelin that is undergoing degeneration or refinement (23–25). Our EM analysis indicates the myelin reporter labels compact myelin and could be used at this level to look at more accurate and detailed analysis of the myelin wrapping and g-ratios of small-caliber axons. In addition, a potential limitation of the reporter is the eventual exclusion of membrane label from compact structures as has been previously reported for myelin protein fusion reporters (49). Nevertheless, the fidelity to examine regenerated myelin indices at light and EM levels makes this model system a potent new tool for observing many of the unanswered questions of the dynamic changes injured myelin may undergo over time.

In conclusion, these studies reveal that remyelination following central insult is a profoundly prolonged process of sheath refinement, leading us to reevaluate our conception of how myelin is regenerated. We demonstrate that, even in the setting of trauma, most regenerated myelin eventually attains remarkably similar physical characteristics to myelin formed during development. Now that we have a clearer understanding of the robust nature of remyelination and the capacity for sheath plasticity, we may also begin to design new studies to evaluate remyelination-directed therapies for spinal cord injury, stroke, and other demyelinating disorders.

Methods

SI Methods provides additional information on surgical procedures and methods.

Animals. A total of 24 *Gt(ROSA)26Sor*$^{tm4(ACTB-tdTomato,-EGFP)Luo}$/J mice (Jackson Labs) were used in this study. All procedures were in accordance with a protocol approved by the Animal Care and Use Committee of the University of Washington.

Virus Production. A Phoenix–Moloney murine leukemia virus expression vector, pLNpCRESN, with Cre recombinase under the control of the NG2 promoter has previously been described and characterized (31). To generate retrovirus, pLNpCRESN was cotransfected with the VSV-G envelope vector into Phoenix-GP

packaging cells (American Type Culture Collection). Infectious virus particles were harvested 48, 72, and 96 h posttransfection and concentrated via ultracentrifugation to 1×10^{10} infectious particles per microliter.

Confocal Microscopy and Quantitative Analysis. Multichannel confocal *z*-series images were generated using a Nikon A1 Confocal System attached to a Ti-E inverted microscope platform. To quantify myelin and axonal dimensions, all mG^+ sheaths within six longitudinal sections containing the lesion from each animal were imaged ($n = 2$ each from ventral, central, and dorsal spinal cord). Quantification was performed by using NIS Elements software (Nikon). Sheath length was measured along NF^+ axons from one $CASPR^+$ paranode to the other. Sheath widths were measured in at least four locations in flattened *z*-stacks and averaged. Basal lamina, but not cell body, was included in SC sheath width measurements. SC sheaths were identified by the presence of an mG^+ soma with $DAPI^+$ nucleus hugging the exterior of the sheath. OL sheaths were identified by the presence of attached thin projections from a satellite $mG^+/DAPI^+$ cell body. NF^+ axonal diameter was measured in at least two locations and averaged. Where NF antibody penetration was weak (typical within the internode in heavily myelinated regions), average width of both CASPR-labeled paranodes was taken as a measure of axonal diameter.

Immunoelectron Microscopy. Tissues were prepared as described previously (28). Briefly, three injured mice were killed and perfused at 3 MPV with ice-cold 3% (wt/vol) paraformaldehyde/0.5% glutaraldehyde. All steps were performed on ice. Coronal sections of spinal cord 80 μm thick were made on a Vibratome. Sections were rinsed in PBS solution, blocked in 2% BSA in PBS solution, and incubated with rabbit anti-GFP (1:500; Millipore) in block for 2 h followed by goat anti-rabbit Qdot 605 (1:100; Invitrogen) for 1 h in block, and rinsed in PBS solution. Some sections were imaged immediately on a confocal microscope to confirm colocalization of GFP with Qdots. Sections were then dehydrated and processed for EM as previously. Ultrathin sections were imaged by using an JEM-1400 transmission electron microscope (JEOL) with a Gatan Ultrascan 1000XP camera.

Statistical Analysis. Statistical significance among groups was determined by one-way ANOVA with Bonferroni multiple comparison posttest for three or more groups or two-tailed, unpaired *t* test for two groups. Pearson correlations were used to determine the relationship between sheath length and axon or total fiber diameter. A CI of 95% and Prism software was used for all comparisons (GraphPad). Results in the text are reported ±SD.

ACKNOWLEDGMENTS. We thank Drs. Stallcup, Trimmer, and Brophy for their generous gifts of antibodies. This work was funded by National Institutes of Health Grant NSO46724 and an endowment through Frank and Penny Webster (to P.J.H.). Confocal microscopy was supported in part by the Mike and Lynn Garvey Cell Imaging Laboratory at the University of Washington Institute for Stem Cell and Regenerative Medicine.

1. Bjartmar C, Yin X, Trapp BD (1999) Axonal pathology in myelin disorders. *J Neurocytol* 28(4-5):383–395.
2. Lappe-Siefke C, et al. (2003) Disruption of Cnp1 uncouples oligodendroglial functions in axonal support and myelination. *Nat Genet* 33(3):366–374.
3. Nave KA (2010) Myelination and support of axonal integrity by glia. *Nature* 468(7321):244–252.
4. Irvine KA, Blakemore WF (2008) Remyelination protects axons from demyelination-associated axon degeneration. *Brain* 131(pt 6):1464–1477.
5. Crang AJ, Gilson J, Blakemore WF (1998) The demonstration by transplantation of the very restricted remyelinating potential of post-mitotic oligodendrocytes. *J Neurocytol* 27(7):541–553.
6. Keirstead HS, Blakemore WF (1997) Identification of post-mitotic oligodendrocytes incapable of remyelination within the demyelinated adult spinal cord. *J Neuropathol Exp Neurol* 56(11):1191–1201.
7. Nishiyama A (1998) Glial progenitor cells in normal and pathological states. *Keio J Med* 47(4):205–208.
8. Tripathi R, McTigue DM (2007) Prominent oligodendrocyte genesis along the border of spinal contusion lesions. *Glia* 55(7):698–711.
9. Dawson MR, Polito A, Levine JM, Reynolds R (2003) NG2-expressing glial progenitor cells: an abundant and widespread population of cycling cells in the adult rat CNS. *Mol Cell Neurosci* 24(2):476–488.
10. Zawadzka M, et al. (2010) CNS-resident glial progenitor/stem cells produce Schwann cells as well as oligodendrocytes during repair of CNS demyelination. *Cell Stem Cell* 6(6):578–590.
11. Nashmi R, Fehlings MG (2001) Changes in axonal physiology and morphology after chronic compressive injury of the rat thoracic spinal cord. *Neuroscience* 104(1):235–251.
12. Smith KJ, Blakemore WF, McDonald WI (1979) Central remyelination restores secure conduction. *Nature* 280(5721):395–396.
13. Fancy SP, Chan JR, Baranzini SE, Franklin RJ, Rowitch DH (2011) Myelin regeneration: A recapitulation of development? *Annu Rev Neurosci* 34:21–43.
14. Guest JD, Hiester ED, Bunge RP (2005) Demyelination and Schwann cell responses adjacent to injury epicenter cavities following chronic human spinal cord injury. *Exp Neurol* 192(2):384–393.
15. Miron VE, Kuhlmann T, Antel JP (2011) Cells of the oligodendroglial lineage, myelination, and remyelination. *Biochim Biophys Acta* 1812(2):184–193.
16. Franklin RJ, Ffrench-Constant C (2008) Remyelination in the CNS: From biology to therapy. *Nat Rev Neurosci* 9(11):839–855.
17. McDonald JW, Howard MJ (2002) Repairing the damaged spinal cord: A summary of our early success with embryonic stem cell transplantation and remyelination. *Prog Brain Res* 137:299–309.
18. Bunge MB, Bunge RP, Ris H (1961) Ultrastructural study of remyelination in an experimental lesion in adult cat spinal cord. *J Biophys Biochem Cytol* 10:67–94.
19. Blakemore WF, Murray JA (1981) Quantitative examination of internodal length of remyelinated nerve fibres in the central nervous system. *J Neurol Sci* 49(2):273–284.
20. Gledhill RF, McDonald WI (1977) Morphological characteristics of central demyelination and remyelination: A single-fiber study. *Ann Neurol* 1(6):552–560.
21. Hagg T, Oudega M (2006) Degenerative and spontaneous regenerative processes after spinal cord injury. *J Neurotrauma* 23(3-4):264–280.
22. Totoiu MO, Keirstead HS (2005) Spinal cord injury is accompanied by chronic progressive demyelination. *J Comp Neurol* 486(4):373–383.
23. Harrison BM, McDonald WI, Ochoa J, Ohlrich GD (1972) Paranodal demyelination in the central nervous system. *J Neurol Sci* 16(4):489–494.
24. Ohlrich GD, McDonald WI (1974) Demyelination in the central nervous system of the cat studied by single fibre isolation. *Proc Aust Assoc Neurol* 11:77–87.
25. Smith PM, Jeffery ND (2006) Histological and ultrastructural analysis of white matter damage after naturally-occurring spinal cord injury. *Brain Pathol* 16(2):99–109.
26. Brill MH, Waxman SG, Moore JW, Joyner RW (1977) Conduction velocity and spike configuration in myelinated fibres: Computed dependence on internode distance. *J Neurol Neurosurg Psychiatry* 40(8):769–774.
27. Waxman SG (1980) Determinants of conduction velocity in myelinated nerve fibers. *Muscle Nerve* 3(2):141–150.
28. Lasiene J, Shupe L, Perlmutter S, Horner P (2008) No evidence for chronic demyelination in spared axons after spinal cord injury in a mouse. *J Neurosci* 28(15):3887–3896.
29. van de Meent H, et al. (1996) New assessment techniques for evaluation of post-traumatic spinal cord function in the rat. *J Neurotrauma* 13(12):741–754.
30. Muzumdar MD, Tasic B, Miyamichi K, Li L, Luo L (2007) A global double-fluorescent Cre reporter mouse. *Genesis* 45(9):593–605.
31. Sellers DL, Maris DO, Horner PJ (2009) Postinjury niches induce temporal shifts in progenitor fates to direct lesion repair after spinal cord injury. *J Neurosci* 29(20):6722–6733.
32. Roe T, Reynolds TC, Yu G, Brown PO (1993) Integration of murine leukemia virus DNA depends on mitosis. *EMBO J* 12(5):2099–2108.
33. McTigue DM, Tripathi R, Wei P (2006) NG2 colocalizes with axons and is expressed by a mixed cell population in spinal cord lesions. *J Neuropathol Exp Neurol* 65(4):406–420.
34. Stegmüller J, Schneider S, Hellwig A, Garwood J, Trotter J (2002) AN2, the mouse homologue of NG2, is a surface antigen on glial precursor cells implicated in control of cell migration. *J Neurocytol* 31(6-7):497–505.
35. Jasmin L, Janni G, Moallem TM, Lappi DA, Ohara PT (2000) Schwann cells are removed from the spinal cord after effecting recovery from paraplegia. *J Neurosci* 20(24):9215–9223.
36. Bunge RP (1968) Glial cells and the central myelin sheath. *Physiol Rev* 48(1):197–251.
37. Gledhill RF, Harrison BM, McDonald WI (1973) Demyelination and remyelination after acute spinal cord compression. *Exp Neurol* 38(3):472–487.
38. Brinkmann BG, et al. (2008) Neuregulin-1/ErbB signaling serves distinct functions in myelination of the peripheral and central nervous system. *Neuron* 59(4):581–595.
39. Fancy SP, et al. (2009) Dysregulation of the Wnt pathway inhibits timely myelination and remyelination in the mammalian CNS. *Genes Dev* 23(13):1571–1585.
40. Blakemore WF (1974) Pattern of remyelination in the CNS. *Nature* 249(457):577–578.
41. Fraher JP, Rossiter JP (1991) Myelin-axon relationships established by rat vagal Schwann cells deep to the brainstem surface. *J Comp Neurol* 304(2):253–260.
42. de Waegh SM, Lee VM, Brady ST (1992) Local modulation of neurofilament phosphorylation, axonal caliber, and slow axonal transport by myelinating Schwann cells. *Cell* 68(3):451–463.
43. Friede RL, Meier T, Diem M (1981) How is the exact length of an internode determined. *J Neurol Sci* 50(2):217–228.
44. Friede RL, Brzoska J, Hartmann U (1985) Changes in myelin sheath thickness and internode geometry in the rabbit phrenic nerve during growth. *J Anat* 143:103–113.
45. Jessen KR, Mirsky R (2005) The origin and development of glial cells in peripheral nerves. *Nat Rev Neurosci* 6(9):671–682.
46. Baumann N, Pham-Dinh D (2001) Biology of oligodendrocyte and myelin in the mammalian central nervous system. *Physiol Rev* 81(2):871–927.
47. Almeida RG, Czopka T, Ffrench-Constant C, Lyons DA (2011) Individual axons regulate the myelinating potential of single oligodendrocytes in vivo. *Development* 138(20):4443–4450.
48. Câmara J, et al. (2009) Integrin-mediated axoglial interactions initiate myelination in the central nervous system. *J Cell Biol* 185(4):699–712.
49. Aggarwal S, et al. (2011) A size barrier limits protein diffusion at the cell surface to generate lipid-rich myelin-membrane sheets. *Dev Cell* 21(3):445–456.